Enhanced spin-torque in double tunnel junctions using a nonmagnetic-metal spacer

C. H. Chen, Y. H. Cheng, C. W. Ko, and W. J. Hsueh

Citation: Applied Physics Letters **107**, 152401 (2015); doi: 10.1063/1.4933101
View online: http://dx.doi.org/10.1063/1.4933101
View Table of Contents: http://scitation.aip.org/content/aip/journal/apl/107/15?ver=pdfcov
Published by the AIP Publishing

Enhanced spin-torque in double tunnel junctions using a nonmagnetic-metal spacer

C. H. Chen, Y. H. Cheng, C. W. Ko, and W. J. Hsueh[a)]
Nanomagnetism Group, Department of Engineering Science and Ocean Engineering, National Taiwan University, 1, Sec. 4, Roosevelt Road, Taipei 10660, Taiwan

(Received 7 July 2015; accepted 1 October 2015; published online 12 October 2015)

This study proposes an enhancement in the spin-transfer torque of a magnetic tunnel junction (MTJ) designed with double-barrier layer structure using a nonmagnetic metal spacer, as a replacement for the ferromagnetic material, which is traditionally used in these double-barrier stacks. Our calculation results show that the spin-transfer torque and charge current density of the proposed double-barrier MTJ can be as much as two orders of magnitude larger than the traditional double-barrier one. In other words, the proposed double-barrier MTJ has a spin-transfer torque that is three orders larger than that of the single-barrier stack. This improvement may be attributed to the quantum-well states that are formed in the nonmagnetic metal spacer and the resonant tunneling mechanism that exists throughout the system. © *2015 AIP Publishing LLC*.
[http://dx.doi.org/10.1063/1.4933101]

Spin-transfer torque (STT) in magnetic tunnel junctions (MTJs) has attracted widespread attention in recent times given the theoretical predictions,[1,2] experimental confirmation,[3–6] and potential applications such as STT magnetic random access memories[7] (STT-MRAM) and spin torque nano-oscillators.[8–10] Improvements in writing (lower switching current) and reading (higher magnetoresistance) of the stored binary data are crucial to the development of STT-MRAM. While first considered for metallic spin valves, STT was soon studied in MTJs, where the spacer between two ferromagnetic electrodes was replaced by insulating barriers such as Al_2O_3 or MgO.[11,12] The critical current densities for a typical tri-layer MTJ consisting of two ferromagnetic layers of CoFeB separated by a nonmagnetic insulator such as MgO are usually on the order of 10^6–10^7 A/cm^2.[12,13]

In nanoelectronics, double- or multi-barrier structures are considered important because of the formation of quantum wells between the barriers, resulting in resonant tunneling effects and leading to many useful applications.[14–17] The tunnel magnetoresistance (TMR) effect in MTJs with different structures, including single-barrier,[18] double-barrier,[19] and multi-barrier[20] stacks, has been observed in several studies. The effect of using a nonmagnetic metal on the TMR ratio has also been investigated.[20–22] For the STT effect in MTJ, improvement of STT using the double-barrier structure of the form F/I/F/I/F has been proposed,[13,23–25] where F and I denote the ferro-magnet and the insulator, respectively. However, a comparison between the traditional double-barrier MTJ (F/I/F/I/F)[13] and the single-barrier MTJ (F/I/F) shows that the STT in the former is approximately only an order of magnitude higher than that in the latter.

In this study, the STT generated in the double-barrier MTJ with the structure F/I/N/I/F is studied, where N stands for the nonmagnetic metal spacer (NMS). However, STT in double-barrier MTJ with a NMS has not been studied before. Our model and simulation results show that the STT in the double-barrier MTJ with the F/I/N/I/F layered configuration can be up to three orders of magnitude higher than that in the single-barrier MTJ, provided the thickness of the nonmagnetic-metal spacer is properly designed.

Initially, we considered an MTJ with a double-barrier structure with two insulators separated by a NMS, with both sides enclosed by the same ferromagnetic electrodes, as shown in Fig. 1(a). This double-barrier MTJ is denoted as F_L/I/N/I/F_R, where $F_{L(R)}$ stands for the ferromagnetic electrode on the left (right) side. The thickness of the left and the right barriers is assumed to be the same in this study. We denote the barrier thickness and the NMS thickness by d_I and d_N, respectively. These layers are nanometers in thickness and electron transport in these layers are nearly ballistic. The MTJ is restricted to be large-area planar junctions, in which the Coulomb blockade effects do not occur. It is assumed that the ferromagnetic electrodes are thick enough to be treated as semi-infinite.[26,27] A bias voltage V is applied between the two ferromagnetic electrodes. The angle between the magnetization of F_L and F_R is denoted by θ. The direction of magnetization for the ferromagnetic electrode on the right side can be changed by electric current and/or magnetic field. There are two local coordinate systems used in this study. The first one with axes x, y, and z is used for the left ferromagnetic electrode, NMS, and insulator. The second coordinate system with axes x', y', and z' is used in the ferromagnetic electrode on the

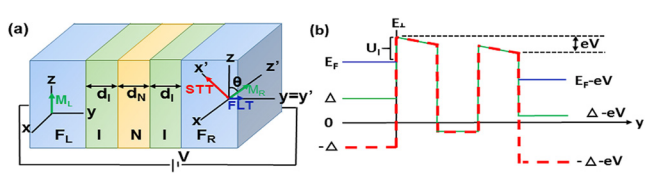

FIG. 1. (a) Schematic picture of a double-barrier MTJ of the form F_L/I/N/I/F_R. M_L and M_R denote the magnetizations of the two ferromagnetic electrodes. STT and FLT are the two components of the spin torque exerted on the right ferromagnetic electrode. (b) The potential profile for spin-up (red dashed line) and spin-down (green solid line) for parallel configuration.

[a)]Author to whom correspondence should be addressed. Electronic mail: hsuehwj@ntu.edu.tw. Tel.: 886-2-3366-5750. FAX: 886-2-2392-9885

right side. The axis z (z') is in the same direction as the magnetization for the left/right electrode. The layers in the MTJ are perpendicular to the y ($=y'$)-axis. It is assumed that the x and x' axes lie in the plane formed by the two magnetizations.

The torque exerted on the right electrode has two components: STT (in-plane torque) and field-like torque (FLT). The STT and FLT exerted per unit square of the F_R layer[27] can be expressed as

$$STT = -\frac{\hbar}{2} J_{s,x'}, \tag{1}$$

and

$$FLT = -\frac{\hbar}{2} J_{s,y'}, \tag{2}$$

where $J_{s,x'}(J_{s,y'})$ is the x'(y')-component of the spin current density. The μth component of the spin current density can be expressed by Eq. (3) based on Ref. 28 as

$$j^s_\alpha(y) = \frac{i\hbar}{2m}\left[\left(\frac{\partial}{\partial y}\Psi^+(y)\right)\sigma_\alpha\Psi(y) - \Psi^+(y)\sigma_\alpha\Psi(y)\right], \tag{3}$$

where $\Psi = \begin{bmatrix}\psi_\uparrow(y)\\ \psi_\downarrow(y)\end{bmatrix}$ and σ_α are the Pauli matrices. Based on the formulation above, the charge current density can now be calculated as

$$j(y) = \frac{e\hbar}{m}\sum_\sigma \psi^*_\sigma\left[\frac{d\psi_\sigma}{dy}\right]. \tag{4}$$

This study uses the parabolic band model, first proposed by Slonczewski,[1,29] to compute electronic transport in magnetic multilayers. The Schrödinger equation for the wave function for spin-up ($\psi_\uparrow$) and spin down ($\psi_\downarrow$) electrons with an electron mass, m, can be written as $\left(-\frac{\hbar^2}{2m}\nabla^2 + U - \vec{\Delta}\cdot\vec{\sigma}\right)\begin{pmatrix}\psi_\uparrow\\ \psi_\downarrow\end{pmatrix} = E\begin{pmatrix}\psi_\uparrow\\ \psi_\downarrow\end{pmatrix}$, where $\vec{\Delta}$ is the molecular field caused by s-d exchange interaction.[29] U is the potential barrier height. The wave functions in layer j can be written as $\psi^\sigma_j(y) = A^\sigma_j e^{ik^\sigma_j(y-y_j)} + B^\sigma_j e^{-ik^\sigma_j(y-y_j)}$, where A^σ_j and B^σ_j are the amplitudes of the waves in the +y and −y directions, respectively. The superscript, $\sigma = \pm 1$ or ($\sigma = \uparrow, \downarrow$), denotes spin-up and spin-down electrons. The potential profile of the barriers becomes trapezoidal when bias is applied, as shown in Fig. 1(b). The first and the second barriers are sliced into N rectangular barriers. The magnitude of the rectangular barriers is $U_n = (U + E_F) - n\cdot eV/N$, where $n = 1, 2, \ldots, N$ denotes the nth rectangular barrier counted from the left to the right. Note that the potential barrier U is measured with reference to the Fermi energy, E_F. The wave vectors in the F_L and F_R layers are $k^\sigma_{F_L} = \sqrt{\frac{2m}{\hbar^2}(E_\perp + \sigma\Delta)}$ and $k^\sigma_{F_R} = \sqrt{\frac{2m}{\hbar^2}(E_\perp + \sigma\Delta - eV)}$, where Δ represents the half of the spin-splitting of the electron band in the ferromagnetic electrodes, and $E_\perp$ is the transverse component of the total electron energy, given by $E_\perp = E - \hbar^2 k^2_{||}/2m$. Therefore, $E_\perp$ is measured with respect to the midpoint between the bottom portions of the two spin sub-bands in the left electrode. In the barrier and the NMS, the wave vectors are $k^\sigma_I = \sqrt{\frac{2m}{\hbar^2}(E_\perp - U_n)}$ and $k^\sigma_N = \sqrt{\frac{2m}{\hbar^2}\left(E_\perp - \frac{eV}{2}\right)}$. At all the boundaries of the system, the wave function and its derivative must be continuous. Since there is a change of the quantization axis at the boundary between the right-hand side insulator and ferromagnet, the boundary condition is expressed as $\psi^\uparrow_I = \psi^\uparrow_{F_R}\cos(\theta/2) + \psi^\downarrow_{F_R}\sin(\theta/2)$ and $\psi^\downarrow_I = -\psi^\uparrow_{F_R}\sin(\theta/2) + \psi^\downarrow_{F_R}\cos(\theta/2)$. Based on these boundary conditions, the transfer matrix of the entire system can be expressed as $T_{total} = \ldots (P_{j-1}M_{j-1}{}^{-1})Q_j(P_jM_j{}^{-1})Q_{j+1}(P_{j+1}M_{j+1}{}^{-1})\ldots$, where $P_j = \begin{pmatrix}P'^\uparrow_j & O\\ O & P'^\downarrow_j\end{pmatrix}$, $Q_j = \begin{pmatrix}Q'_j & W_j\\ -W_j & Q'_j\end{pmatrix}$, and $M = \begin{pmatrix}M'^\uparrow_j & O\\ O & M'^\downarrow_j\end{pmatrix}$. The submatrix P'^σ_j in P_j is defined as $P'^\sigma_j = \begin{pmatrix}1 & 1\\ ik^\sigma_j/m & -ik^\sigma_j/m\end{pmatrix}$. O is the 2 × 2 null matrix. The submatrix Q'_j and W_j are defined as $Q_j = \begin{pmatrix}\cos(\theta/2) & 0\\ 0 & \cos(\theta/2)\end{pmatrix}$ and $W_j = \begin{pmatrix}\sin(\theta/2) & 0\\ 0 & \sin(\theta/2)\end{pmatrix}$, respectively. The submatrix M'^σ_j in M is defined as $M'^\sigma_j = \begin{pmatrix}\exp(ik^\sigma_j d_j) & \exp(-ik^\sigma_j d_j)\\ (ik^\sigma_j/m)\exp(ik^\sigma_j d_j) & -(ik^\sigma_j/m)\exp(-ik^\sigma_j d_j)\end{pmatrix}$. Based on the transfer matrix method, the amplitude of the electron wave function and the current density can be solved numerically. The total spin current density[30] in the zero temperature limit is

$$J^s_\mu(y) = \frac{4\pi^2 m^2}{h^4}\left[\sum_\sigma \int_{-\sigma\Delta}^{E_F - eV} d\varepsilon_\perp \frac{eV}{k_{l\sigma}(\varepsilon_\perp)} j^s_\mu(y,\varepsilon_\perp) + \int_{E_F - eV}^{E_F} d\varepsilon_\perp \frac{E_F - \varepsilon_\perp}{k_{l\sigma}(\varepsilon_\perp)} j^s_\mu(y,\varepsilon_\perp)\right]. \tag{5}$$

In order to compute the charge current density, the quantity j^s_μ should be replaced by j in Eq. (4).

The relevant parameters for iron are Fermi energy $E_F = 2.62\,eV$ and spin-splitting energy $\Delta = 1.96\,eV$, which have been widely used in the modeling of MTJ.[27] The charge current density and the STT as a function of the thickness of the NMS for three different spin-splitting energies are shown in Fig. 2. Different spin-splitting energies are used in order to understand their effect on spin torque and charge current density. The parameter for Al_2O_3 is used for the insulating layer. The barrier height for the Fe/Al_2O_3 junction is commonly assumed to be equal to $U_I = 1.5\,eV$.[27] The thickness of the barrier is chosen to be relatively thin ($d_I = 0.5\,nm$), in order to obtain a large spin torque. A bias voltage of $V = 0.5\,V$ is applied to the structure. In this case, the electrons tunnel from the left electrode to the right one. As shown in Fig. 2(a), the charge current density is strongly influenced by the thickness of the NMS, d_N. The current oscillates as d_N increases. Several peaks can be seen in the figure. For thicker d_N, the magnitude of these peaks decreases while their width gets broader. For the three different values of Δ, the location of all the different peaks are quite close to each other. The peak value of charge current density is higher for larger Δ. The plot of the STT as a function of d_N also shows several peaks, the height of which

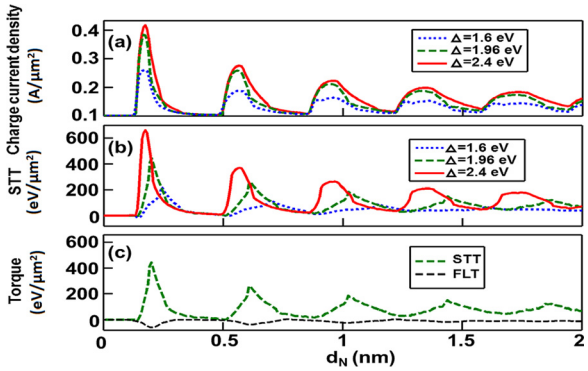

FIG. 2. Trend of the (a) charge current density and (b) STT as a function of the thickness of the NMS (d_N), for three different Δ. (c) Trend of the STT and FLT as a function of the thickness of the NMS for $\Delta = 1.96$ eV. The other parameters used for the simulation are → Fermi energy, $E_F = 2.62$ eV, height of the insulating barrier, $U_I = 1.5$ eV, bias voltage, $V = 0.5$ V, angle between the magnetization of the two ferromagnetic electrodes, $\theta = \pi/2$, and barrier thickness, $d_I = 0.5$ nm.

decreases as d_N increases, as shown in Fig. 2(b). The magnitude of these peaks also decreases, while their width increases for increasing d_N. It is to be noted that the magnitude of these peaks is proportional to the magnitude of Δ. However, their location is obviously different for different values of Δ. Only for the largest spin-splitting energy of $\Delta = 2.4$ eV considered here, the location of the peaks of the STT and charge current density is relatively close.

For $d_N = 0$ nm, our designed stack becomes a traditional single-barrier MTJ. Our calculation results are quite consistent with previous theoretical studies.[26,27] Moreover, these studies have been shown to agree well with experiment.[6] The magnitude of the STT is 0.2, 0.1, and 0.05 eV/μm^2 for $\Delta = 1.6$, 1.96, and 2.4 eV, respectively. Compared with the single-barrier MTJ, the STT in the double-barrier MTJ is significantly enhanced when the thickness of the NMS is properly designed. For instance, the STT of the double-barrier structure with $d_N = 0.6$ nm for $\Delta = 1.96$ eV is about 200 eV/μm^2, which is about 2000 times the value for the single-barrier structure. It is to be expected that the periodic oscillation of the STT as d_N increases is related to the quantum-well states that are formed in the non-magnetic metals and the resonant tunneling mechanism throughout the stack.[21] Figure 2(c) shows the FLT and STT of the double-barrier MTJ for $\Delta = 1.96$ eV. It is found that the STT exerted on the right electrode plays a dominant role in the magnetization reversal phenomenon in this double-barrier MTJ.

Next, we investigate the bias dependence of the charge current density and STT for $d_N = 0$ nm, $d_N = 0.6$ nm, and $d_N = 0.9$ nm, as shown in Fig. 3. The spin-splitting energy used in Fig. 3 is $\Delta = 1.96$ eV. Double-barrier junctions with $d_N = 0.6$ nm and $d_N = 0.9$ nm are investigated in detail, since they correspond to the locations of large and small STT, respectively, as can been seen in Fig. 2(b). The magnitude of the current for double-barrier junctions is quite large compared with that of the single-barrier junction. For $|V| < (>)$ lower (greater) than 0.5 V, the current for $d_N = 0.6$ nm is larger (smaller) than the one for $d_N = 0.9$ nm. On the other hand, the STT for the single-barrier junction is quite small compared to that for the double-barrier junctions, as shown in Fig. 3(b). In other words, a smaller bias voltage is required to achieve the

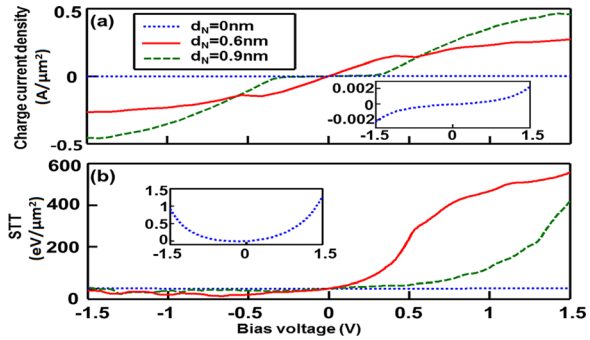

FIG. 3. Bias dependence of the (a) charge current density and (b) STT for three different thicknesses of the NMS. The inset in each figure shows an enlarged view of the plot for $d_N = 0$ nm, corresponding to the singe-barrier case. The other parameters of the junction are the same as those in Fig. 2, except that $\Delta = 1.96$ eV.

same STT that is achieved by the single-barrier MTJ. For positive bias, the STT for the junctions with $d_N = 0.6$ nm is larger than the one with $d_N = 0.9$ nm. For negative bias, although the STT is not as large as the one at positive bias for double-barrier MTJ, it is still larger than the STT of the single-barrier junction. In summary, the STT can be enhanced by using double-barrier junctions with the right thickness for the NMS.

Next, we study the effect of the angle θ between the magnetic moments of the electrodes on the STT and charge current density for $d_N = 0$ nm, $d_N = 0.6$ nm, and $d_N = 0.9$ nm, as shown in Fig. 4. For the STT of the single-barrier MTJ ($d_N = 0$ nm), as one might expect, the torque is zero in the collinear configuration and reaches a maximum absolute value for $\theta = \pi/2$ and $\theta = 3\pi/2$, i.e., when the magnetic moments of the electrodes are oriented perpendicularly.[27] For the case of the double-barrier MTJ, the features of the STT are quite similar to the single-barrier MTJ, except that the magnitude of the torque is different. For $d_N = 0.9$ nm, the STT is two orders of magnitude larger than that of the single-barrier MTJ. When comparing this with $d_N = 0.6$ nm, the STT value shows a further increase of one order of magnitude. Figures 4(b)–4(d) show the charge current densities for $d_N = 0$ nm, $d_N = 0.6$ nm, and $d_N = 0.9$ nm, respectively. Considering the single-barrier MTJ ($d_N = 0$ nm), the charge current density is maximal in the parallel configuration and monotonically decreases when

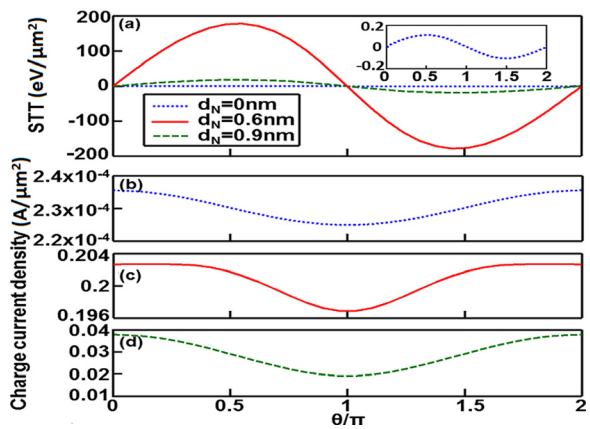

FIG. 4. Plot of (a) STT as a function of θ for three different thickness values of d_N. The inset shows an enlarged view of the plot for $d_N = 0$ nm. In (b)–(d), the charge current density as a function of θ for (b) $d_N = 0$ nm, (c) $d_N = 0.6$ nm, and (d) $d_N = 0.9$ nm is presented. The parameters are the same as those used in Fig. 2, except that $\Delta = 1.96$ eV.

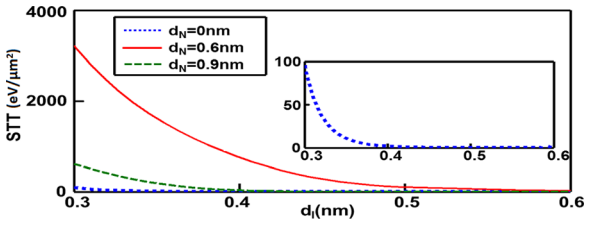

FIG. 5. Trend of the STT as a function of the barrier thickness for the same three different values of d_N. The parameters are the same as those used in Fig. 2, except that $\Delta = 1.96$ eV. The inset is a partially zoomed-in view of the trend corresponding to $d_N = 0$ nm.

magnetic moments rotate towards the anti-parallel configuration. The same trend is observed for the double-barrier MTJ with $d_N = 0.6$ nm and $d_N = 0.9$ nm. However, the charge current density of the double-barrier structure with $d_N = 0.6$ nm ($d_N = 0.9$ nm) is three (two) orders of magnitude larger than that of the single-barrier structure.

Besides the thickness of the NMS, the effect of the barrier thickness on the STT is also studied, as shown in Fig. 5. Similar to the case of the single-barrier MTJ, the STT decreases gradually for increasing barrier thicknesses. However, the STT for the double-barrier MTJ is higher than that for the single-barrier MTJ, especially when the thickness of the barrier is small. Further comparison between the two cases of double-barrier MTJ, with $d_N = 0.6$ nm and $d_N = 0.9$ nm, shows again that a proper choice of the NMS is crucial to achieve large STT.

In conclusion, enhancement of the STT in double-barrier MTJs using NMS is proposed. Interestingly, the STT and the charge current density of this double-barrier structure show up to two orders of magnitude improvement when compared with the traditional double-barrier MTJs and three orders of magnitude enhancement with reference to the single-barrier MTJs, given the same applied voltage, if the thickness of the NMS is properly designed. This improvement in characteristics can be attributed to the quantum-well states that are formed in the NMS and the resonant tunneling mechanism through the entire stack. The bias dependence of the STT for the investigated structure is found to be asymmetric. With increasing barrier thickness, the STT shows a monotonically decay trends.

The authors acknowledge the support provided by the Ministry of Science and Technology of Taiwan, under Grant Nos. MOST 104-3113-E-002-001 and MOST 103-2221-E-002-118.

[1]J. C. Slonczewski, J. Magn. Magn. Mater. **159**, L1 (1996).
[2]L. Berger, Phys. Rev. B **54**, 9353 (1996).
[3]S. I. Kiselev, J. C. Sankey, I. N. Krivorotov, N. C. Emley, R. J. Schoelkopf, R. A. Buhrman, and D. C. Ralph, Nature **425**, 380 (2003).
[4]J. A. Katine, F. J. Albert, R. A. Buhrman, E. B. Myers, and D. C. Ralph, Phys. Rev. Lett. **84**, 3149 (2000).
[5]C. Wang, Y. T. Cui, J. Z. Sun, J. A. Katine, R. A. Buhrman, and D. C. Ralph, Phys. Rev. B **79**, 224416 (2009).
[6]H. Kubota, A. Fukushima, K. Yakushiji, T. Nagahama, S. Yuasa, K. Ando, H. Maehara, Y. Nagamine, K. Tsunekawa, D. D. Djayaprawira, N. Watanabe, and Y. Suzuki, Nat. Phys. **4**, 37 (2008).
[7]L. Thomas, G. Jan, S. Le, and P.-K. Wang, Appl. Phys. Lett. **106**, 162402 (2015).
[8]V. Sluka, A. Kákay, A. M. Deac, D. E. Bürgler, C. M. Schneider, and R. Hertel, Nat. Commun. **6**, 6409 (2015).
[9]S. Kaka, M. R. Pufall, W. H. Rippard, T. J. Silva, S. E. Russek, and J. A. Katine, Nature **437**, 389 (2005).
[10]N. Locatelli, V. Cros, and J. Grollier, Nat. Mater. **13**, 11 (2014).
[11]Y. Huai, F. Albert, P. Nguyen, M. Pakala, and T. Valet, Appl. Phys. Lett. **84**, 3118 (2004).
[12]Z. Diao, D. Apalkov, M. Pakala, Y. Ding, A. Panchula, and Y. Huai, Appl. Phys. Lett. **87**, 232502 (2005).
[13]N. N. Mojumder, C. Augustine, D. E. Nikonov, and K. Roy, J. Appl. Phys. **108**, 104306 (2010).
[14]C. H. Chang, C. W. Tsao, and W. J. Hsueh, New J. Phys. **16**, 113069 (2014).
[15]H. S. Nguyen, D. Vishnevsky, C. Sturm, D. Tanese, D. Solnyshkov, E. Galopin, A. Lemaître, I. Sagnes, A. Amo, G. Malpuech, and J. Bloch, Phys. Rev. Lett. **110**, 236601 (2013).
[16]R. S. Liu, S.-H. Yang, X. Jiang, X. G. Zhang, C. Rettner, L. Gao, T. Topuria, P. M. Rice, W. Zhang, C. M. Canali, and S. S. P. Parkin, Phys. Rev. B **87**, 024411 (2013).
[17]Y. H. Cheng, C. H. Chang, C. H. Chen, and W. J. Hsueh, Phys. Rev. A **90**, 023830 (2014).
[18]S. Yuasa, T. Nagahama, A. Fukushima, Y. Suzuki, and K. Ando, Nat. Mater. **3**, 868 (2004).
[19]R. Liu, S.-H. Yang, X. Jiang, T. Topuria, P. M. Rice, C. Rettner, and S. Parkin, Appl. Phys. Lett. **100**, 012401 (2012).
[20]C. H. Chen and W. J. Hsueh, Appl. Phys. Lett. **104**, 042405 (2014).
[21]M. Wilczynski and J. Barnas, J. Magn. Magn. Mater. **221**, 373 (2000).
[22]S. Yuasa, T. Nagahama, and Y. Suzuki, Science **297**, 234 (2002).
[23]Z. Diao, A. Panchula, Y. Ding, M. Pakala, S. Wang, Z. Li, D. Apalkov, H. Nagai, A. Driskill-Smith, L.-C. Wang, E. Chen, and Y. Huai, Appl. Phys. Lett. **90**, 132508 (2007).
[24]I. Theodonis, A. Kalitsov, and N. Kioussis, J. Magn. Magn. Mater. **310**, 2043 (2007).
[25]A. Vedyayev, N. Ryzhanova, B. Dieny, and N. Strelkov, Phys. Lett. A **355**, 243 (2006).
[26]I. Theodonis, N. Kioussis, A. Kalitsov, M. Chshiev, and W. H. Butler, Phys. Rev. Lett. **97**, 237205 (2006).
[27]M. Wilczyński, J. Barnaś, and R. Świrkowicz, Phys. Rev. B **77**, 054434 (2008).
[28]V. K. Dugaev, V. R. Vieira, P. D. Sacramento, J. Barnaś, M. A. N. Araújo, and J. Berakdar, Phys. Rev. B **74**, 054403 (2006).
[29]J. C. Slonczewski, Phys. Rev. B **39**, 6995 (1989).
[30]M. Wilczyński, J. Magn. Magn. Mater. **325**, 94 (2013).